

Comparison of optical model results from a microscopic Schrödinger approach to nucleon-nucleus elastic scattering with those from a global Dirac phenomenology.

P. K. Deb* and B. C. Clark†

Department of Physics, The Ohio State University, Columbus, OH 43210, U.S.A.

S. Hama‡

Hiroshima University of Economics, Hiroshima 731-0192, Japan

K. Amos§ and S. Karataglidis¶

School of Physics, The University of Melbourne, Victoria 3010, Australia

E. D. Cooper**

University College of the Fraser Valley, Abbotsford, BC 72S 7M8 Canada

(Dated: December 3, 2018)

Abstract

Comparisons are made between results of calculations for intermediate energy nucleon-nucleus scattering for ^{12}C , ^{16}O , ^{40}Ca , ^{90}Zr , and ^{208}Pb , using optical potentials obtained from global Dirac phenomenology and from a microscopic Schrödinger model. Differential cross sections and spin observables for scattering from the set of five nuclei at 65 MeV and 200 MeV have been studied to assess the relative merits of each approach. Total reaction cross sections from proton-nucleus and total cross sections from neutron-nucleus scattering have been evaluated and compared with data for those five targets in the energy range 20 MeV to 800 MeV. The methods of analyses give results that compare well with experimental data in those energy regimes for which the procedures are suited.

PACS numbers: 24.10.Ht, 21.30.Fe, 25.40.Cm, 25.40.Dn, 21.60.Cs

*Electronic address: pdeb@mps.ohio-state.edu

†Electronic address: bcc@mps.ohio-state.edu

‡Electronic address: sn-hama@hue.ac.jp

§Electronic address: amos@physics.unimelb.edu.au

¶Electronic address: kara@physics.unimelb.edu.au

**Electronic address: tim.cooper@ucfv.ca

I. INTRODUCTION

Traditionally the physics of the interaction of a nucleon with a nucleus has been represented by an optical potential. Once that potential is specified, and by its use also the scattering matrix, all observables may be calculated. For intermediate energies there have been a number of methods of calculating the optical potential, the most successful of which have been the global Dirac phenomenology (DP) [1] and a microscopic Schrödinger model [2] in coordinate space identified in the literature as the g -folding method.

The global DP approach is the outgrowth of the seminal work by Walecka and his group [3] with a second order reduction of the Dirac equation leading to Schrödinger equivalent equations. Potentials in those equations have been found with which good fits to elastic nucleon-nucleus scattering data result [1] and more recently, using a global DP, very good fits have been found for nucleon energies ranging from 20 MeV to 1040 MeV [4]. Such potentials are utilitarian for use in analyses of other data. In the g -folding approach, optical potentials are obtained by first deriving an effective NN interaction in-medium from a realistic free nucleon-nucleon (NN) potential. That effective interaction is then folded with a suitable representation of the density matrix of the target nucleus.

Both approaches have had success. Not only have they given good predictions of differential cross sections but also they have reproduced spin and integral observables [2, 4, 5, 6]. A specific example of the success with the g -folding method has been its use in analyzing 200 MeV data from ^{208}Pb . Excellent results were obtained with structure given by a Skyrme-Hartree-Fock (SHF) model [7] for the ground state that is consistent with the Friedman-Pandaharipande neutron equation of state [8]. The global DP approach, based on the relativistic impulse approximation (RIA), fits the data well when proton and neutron densities, their root-mean-square radii, and the neutron skin thickness, all are credible. Targets of ^{40}Ca , ^{48}Ca and ^{208}Pb were considered [9].

However, the two models fundamentally are different. The global DP model is dependent on the fitting of data to determine the parameters in the assumed potentials. Conversely, the microscopic Schrödinger model is dependent upon obtaining realistic effective NN interactions and upon the quality of the model chosen for the structure of the ground state of the target. A complex non-local optical potential results. Of course one can find a local equivalent to this but there is no *a priori* reason to assume that the (non-relativistic) potential deduced from the Dirac reduction resembles, in any way, that equivalent local potential.

Yet, to date, only one real comparison [10] has been made simultaneously of the results from the Dirac and the g -folding approaches for nucleon projectiles, and that for the ^{208}Pb nucleus and 100, 200, and 300 MeV nucleons. Also, an earlier comparison of the Dirac and the then favored phenomenological Schrödinger models revealed problems inherent in the latter [5]. The phenomenological Schrödinger model usually assumes a simple local Woods-Saxon form of the optical potential. Such an approach often fails to reproduce spin observables well enough due to assumptions made in defining the spin-orbit potential. However, a more complex phenomenological (local) Schrödinger model has been developed recently [11], with a global parameter specification, that does replicate very well a large data set for energies 0 to 200 MeV.

The past successes of the two model prescriptions suggest that both may be preset in a way that allows a fair comparison between them, particularly when the results are predictions in that no *a posteriori* adjustments to any facet of the base model details are considered. With that in mind, the prime purpose of this paper is to compare in detail results obtained

from the global DP model with those from the g -folding model for proton scattering. First we report on results of predictions of angular observables for elastic scattering of 65 MeV and of 200 MeV protons from ^{12}C , ^{16}O , ^{40}Ca , ^{90}Zr , and ^{208}Pb . For all cases, the results of the calculations made were plotted before any data was added. We also consider integral observables for both proton and neutron scattering for energies to 800 MeV to evaluate the isospin dependence of the potentials.

In this paper, the formalism of the microscopic g -folding and that of the global DP approach are discussed briefly in Sect. II and the results are presented in Sect. III. In the latter there are two subsections. In the first of those, the results of calculations at 65 MeV and 200 MeV of differential cross sections and of spin observables, A_y and Q , are compared with data. In the second, predictions of reaction and total reaction cross sections made using both methods are compared with data for the five nuclei selected to span the mass range. Conclusions that may be drawn are given thereafter in Sect. IV.

II. MODELS OF THE NUCLEON-NUCLEUS OPTICAL POTENTIAL

As detailed presentations of the two model prescriptions of interest have been published [1, 2, 4], only salient features are given herein.

A. The microscopic g -folding model

To form the g -folding model optical potential it is assumed that pairwise interactions between the projectile nucleon and each bound nucleon as prescribed by a large basis model of the target suffice. Thus, in the g -folding approach [2], no phenomenological form for the potential is assumed nor is that potential derived from any other phenomenological potential. Instead the method begins with the g -matrices of a realistic NN potential; those g -matrices being solutions of the Brueckner-Bethe-Goldstone equations in infinite nuclear matter,

$$g_{LL'}^{JST}(p', p; k, K, k_F) = V_{LL'}^{JST}(p, p') + \frac{2}{\pi} \sum_l \int_0^\alpha V_{Ll}^{JST}(p', q) \times \left\{ \frac{\bar{Q}(q, K, k_f)}{\bar{E}(k, K, k_f) - \bar{E}(q, K, k_f) + i\epsilon} \right\} g_{lL'}^{(JST)}(q, p; k, K, k_F) q^2 dq, \quad (1)$$

in which $\bar{Q}(q, K, k_f)$ is an angle-averaged Pauli operator with an average center-of-mass momentum K . The energies, \bar{E} , in the denominator are single particle values within an averaged field [2]. Such equations are solved for 32 NN channels, for Fermi momenta (k_F) up to densities 1.5 times the nuclear density, and for many energies (k found from E with relativistic kinematics) to 300 MeV using the Bonn-B NN potential [12] as the starting interaction for the calculations.

To form optical potentials in coordinate space then necessitates a mapping of those g -matrices onto Bessel transforms of a complex NN effective interaction. That has been made with particular emphasis placed upon reproduction of the on-shell values of the g -matrices. The effective interaction is the mix of sets of Yukawa function form factors for central, two-nucleon spin-orbit, and tensor operators that can be used in the code DWBA98 [13]. The density of the input structure for the target ground state is used to select what values of the complex and energy dependent strengths of the effective interaction are used in the

folding process. When folded with an appropriate ground state density of the target, the microscopic optical potential is obtained naturally, incorporating Pauli blocking and density dependences. The (coordinate space) potential contains both direct and exchange parts; the latter arising from antisymmetrization of the projectile and bound state nucleon wave functions. Consequently the potential is fully nonlocal. As formulated [2], there are no parameters in the model to adjust *a posteriori*. All results then are obtained from a single (predictive) calculation. For energies at which this theory is applicable, much success has been achieved predicting the observables from proton-nucleus scattering for a number of nuclei [2].

Formally, and ignoring complications of spin interactions and expectations, we seek solutions of the Schrödinger equations of the form

$$\left[\frac{\hbar^2}{2\mu} \nabla^2 - V_c(r) + E \right] \Psi(\mathbf{r}) = \int U(\mathbf{r}, \mathbf{r}'; E) \Psi(\mathbf{r}') d\mathbf{r}' , \quad (2)$$

where \mathbf{r}, \mathbf{r}' are relative NA coordinates, $V_c(r)$ is a Coulomb interaction and $U(\mathbf{r}, \mathbf{r}')$ is the optical potential. In practice, such potentials, or their underlying multipoles, are not evaluated specifically when DWBA98 is used. However, it is useful to consider $U(\mathbf{r}, \mathbf{r}')$ and how it may be formed to note how the target structure enters the process. Consider the overlaps which lead to $U(\mathbf{r}, \mathbf{r}')$, i.e.

$$U_{pA}(0, 1) = \left(\Psi_{gs}(1, 2, \dots, A) \left| \sum_{n=1}^A g_{eff}(0n) \right| \Psi_{gs}(1, 2, \dots, A) \right) = (\Psi_{gs} | A g_{eff}(01) | \Psi_{gs}) , \quad (3)$$

where ‘0’ denotes the projectile coordinates, and as all nucleons in the target are equivalent, we have chosen a specific entry (‘1’). By so doing we can make use of a cofactor expansion of the nuclear many-body (ground) state,

$$|\Psi(1, 2, \dots, A)\rangle = \frac{1}{\sqrt{A}} \sum_{\alpha m} |\varphi_{\alpha m}(1)\rangle \underline{a_{\alpha m} |\Psi(1, 2, \dots, A)\rangle} . \quad (4)$$

Here α specifies the quantum number set $\{n, l, j, \zeta\}$ where ζ is the isospin projection. Then, as the underlined factor in Eq. (4) is independent of coordinate ‘1’,

$$U_{pA}(0, 1) = \sum_{\alpha m \alpha' m'} \langle \Psi | a_{\alpha' m'}^\dagger a_{\alpha m} | \Psi \rangle (\varphi_{\alpha' m'}(1) | g_{eff}(10) \{ |\varphi_{\alpha m}(1)\rangle - |\varphi_{\alpha m}(0)\rangle \} , \quad (5)$$

when the required antisymmetry with projectile and struck nucleon is taken into account.

The many-body reduced matrix elements of the particle-hole operator pairs are the OB-DME [2]. Usually for elastic scattering they are just the nucleon shell occupancies of the target, η_α . Thus such occupancies, the single nucleon bound (SP) states, and the effective interactions $g_{eff}(01)$, define the optical potential in this approach, as

$$U(\mathbf{r}_1, \mathbf{r}_2; E) = \sum_{\alpha m} \eta_\alpha \left[\delta(\mathbf{r}_1 - \mathbf{r}_2) \int \varphi_{\alpha m}^*(\mathbf{s}) U^D(R_{1s}, E) \varphi_{\alpha m}(\mathbf{s}) ds \right. \\ \left. + \varphi_{\alpha m}^*(\mathbf{r}_1) U^{Ex}(R_{12}, E) \varphi_{\alpha m}(\mathbf{r}_2) \right] , \quad (6)$$

where $R_{12} = |\mathbf{r}_1 - \mathbf{r}_2|$, and U^D and U^{Ex} are appropriate combinations of components of the effective interaction for the direct and exchange contributions to the optical potential respectively [2].

B. Global DP optical model potentials

A second-order reduction of the Dirac equation for nucleon-nucleus leads to a Schrödinger-equivalent equation that has physically correct, effective, central and spin-orbit potentials. Symmetry allows one to have Lorentz scalar, S, Lorentz vector, V, and tensor, T potentials which, collectively, are termed SVT potentials. However, the tensor force can always be replaced in a phase equivalent way by an effective relativistic potential of just scalar and vector parts, and as our approach is phenomenological, we consider the global DP using scalar-vector (SV) potentials, together with the Coulomb potential. Solutions of those Schrödinger-equivalent equations have given S -matrices with which observables have been predicted very well [14]. In the SV, the real vector potential is large and repulsive while the real scalar potential is somewhat larger and attractive. The imaginary vector potential is attractive and the imaginary scalar is repulsive. The Dirac equation so structured is suitable for simultaneous analyses of proton-nucleus and neutron-nucleus scattering data for incident energies up to several GeV.

The scalar-vector (SV) model of global DP that has been fit to the elastic proton-nucleus scattering observables [4] takes the form

$$U(r, E, A) = V^v(E, A) f^v(r, E, A) + V^s(E, A) f^s(r, E, A) \\ + iW^v(E, A) g^v(r, E, A) + iW^s(E, A) g^s(r, E, A), \quad (7)$$

The superscripts v and s refer to volume and surface peaked terms respectively. The ‘‘COSH’’ form [4] is used in this paper, *viz.*

$$f^v = \frac{\{\cosh [R(E, A)/a(E, A)] - 1\}}{\{\cosh [R(E, A)/a(E, A)] + \cosh [r/a(E, A)] - 2\}}, \\ f^s = \frac{\{\cosh [R(E, A)/a(E, A)] - 1\} \{\cosh [r/a(E, A)] - 1\}}{\{\cosh [R(E, A)/a(E, A)] + \cosh [r/a(E, A)] - 2\}^2}. \quad (8)$$

Similar forms have been taken for g^v and g^s . Thus the optical potential consists of scalar and vector terms each having real and imaginary parts. In the global analyses [4] the eight strength parameters varied with the proton center of mass energy E (in MeV) and with the atomic mass of the target A . The results can be represented by polynomials,

$$V^v(E, A) = v_0 + \sum_{m=1}^4 v_m x^m + \sum_{n=1}^3 v_{n+4} y^n + v_8 xy + v_9 x^2 y + v_{10} xy^2, \quad (9)$$

where $x = 1000/E$ and $y = A/(A+20)$. We have used the same form for all other potentials $V^s(E, A)$, $W^v(E, A)$, and $W^s(E, A)$. But the scalar and vector potentials, and their real and imaginary parts, all may have different geometry parameter values, the energy and mass dependence of which can be expressed by

$$R = A^{1/3} \left[r_0 + \sum_{m=1}^4 r_m x^m + \sum_{n=1}^3 r_{n+4} y^n + r_8 xy + r_9 x^2 y + r_{10} xy^2 \right], \\ a = a_0 + \sum_{m=1}^4 a_m x^m + \sum_{n=1}^3 a_{n+4} y^n + a_8 xy + a_9 x^2 y + a_{10} xy^2. \quad (10)$$

There are many parameters in this specification which have been defined suitably by using a large data set in a search process. In the global DP calculations we use the recoil correction given by Cooper and Jennings [15].

C. Phase shifts, S -matrices, and observables

Irrespective of how the NA optical potential is specified, the objective of its use is to define the scattering (S)-matrix, or equivalently the (complex) phase shifts $\delta_l^\pm(k)$. With superscripts (\pm) identifying $j = l \pm 1/2$, these relate by

$$S_l^\pm(k) = e^{2i\delta_l^\pm(k)} = \eta_l^\pm(k)e^{2i\Re[\delta_l^\pm(k)]} \quad \text{where} \quad \eta_l^\pm(k) = |S_l^\pm(k)| = e^{-2\Im[\delta_l^\pm(k)]}. \quad (11)$$

With $E \propto k^2$, integral observables for neutrons, namely the total elastic, total reaction (absorption), and total cross sections then are given by

$$\begin{aligned} \sigma_{\text{el}}(E) &= \frac{\pi}{k^2} \sum_{l=0}^{\infty} \left\{ (l+1) |S_l^+(k) - 1|^2 + l |S_l^-(k) - 1|^2 \right\}, \\ \sigma_{\text{R}}(E) &= \frac{\pi}{k^2} \sum_{l=0}^{\infty} \left\{ (l+1) [1 - \eta_l^+(k)^2] + l [1 - \eta_l^-(k)^2] \right\}, \end{aligned}$$

and

$$\begin{aligned} \sigma_{\text{TOT}}(E) &= \sigma_{\text{el}}(E) + \sigma_{\text{R}}(E) \\ &= \frac{2\pi}{k^2} \sum_{l=0}^{\infty} \left\{ (l+1) [1 - \eta_l^+(k) \cos(2\Re[\delta_l^+(k)])] + l [1 - \eta_l^-(k) \cos(2\Re[\delta_l^-(k)])] \right\} \end{aligned} \quad (12)$$

respectively. Note that the Coulomb interaction means that only total reaction cross sections (formed by a modification of the above) can be measured from proton scattering.

To evaluate angular observables, and specifically the differential cross sections and analyzing powers, one need form the scattering amplitudes which, for nucleon elastic scattering are then 2×2 matrices in the nucleon spin space having the form,

$$f(\theta) = A(\theta) + iB(\theta)\boldsymbol{\sigma} \cdot \hat{\mathbf{n}}, \quad (13)$$

where, in terms of the S -matrix elements [16],

$$\begin{aligned} A(\theta) &= \frac{1}{2ik} \sum_{l=0}^{\infty} \left\{ (l+1) [S_l^+(k) - 1] + l [S_l^-(k) - 1] \right\} P_l(\theta), \\ B(\theta) &= -\frac{1}{2ik} \sum_{l=1}^{\infty} [S_l^+(k) - S_l^-(k)] P_l^1(\theta). \end{aligned} \quad (14)$$

From these (complex) amplitudes, and with the quantization axis normal to the scattering plane, the (elastic scattering) differential cross section, analyzing power, and spin rotation are defined by

$$\begin{aligned} \frac{d\sigma}{d\Omega} &= |A(\theta)|^2 + |B(\theta)|^2 \\ A_y(\theta) &= \frac{2\Im[A^*(\theta)B(\theta)]}{d\sigma/d\Omega} \\ Q(\theta) &= \frac{2\Re[A^*(\theta)B(\theta)]}{d\sigma/d\Omega}. \end{aligned} \quad (15)$$

The g -folding model results have been obtained using the DWBA98 code [13] which evaluates scattering amplitudes using a helicity formalism [2]. Those scattering amplitudes $\hat{A}(\theta), \hat{B}(\theta)$ relate to $A(\theta), B(\theta)$ by a unitary transformation involving the rotation matrices $\{\mathbf{d}^{\frac{1}{2}}(\theta)\}$ under which the cross section and analyzing power are invariant, in that

$$\begin{aligned} \frac{d\sigma}{d\Omega} &= |A(\theta)|^2 + |B(\theta)|^2 \equiv |\hat{A}(\theta)|^2 + |\hat{B}(\theta)|^2 \\ A_y(\theta) &= \frac{2\Im [\hat{A}^*(\theta)\hat{B}(\theta)]}{d\sigma/d\Omega} \end{aligned} \quad (16)$$

but the spin rotation becomes

$$Q(\theta) = \frac{1}{d\sigma/d\Omega} \left[\left(|\hat{A}(\theta)|^2 - |\hat{B}(\theta)|^2 \right) \sin(\theta) + \left(2\Re [\hat{A}^*(\theta)\hat{B}(\theta)] \right) \cos(\theta) \right]. \quad (17)$$

III. RESULTS AND DATA COMPARISONS

We have chosen five nuclei for study. They are ^{12}C , ^{16}O , ^{40}Ca , ^{90}Zr , and ^{208}Pb . Not only do they span a large range of target mass and ground state isospin, but also some have been described by mean fields derived from large space structure studies which suit comparison of scattering models.

All microscopic model results we show have been evaluated using the DWBA98 program [13], input to which are the density dependent and complex effective NN interactions described earlier. Other input to DWBA98 are the ground state occupancies (OBDME) and the associated SP functions; both of which are defined from nuclear structure calculations. The structures we have used for each nucleus in the g -folding calculations are

- ^{12}C : For this, the lightest mass nucleus we consider, a no-core shell model calculation [17] in the full $(0+2)\hbar\omega$ space defined its ground state. The WBT interaction of Warburton and Brown [18] was used. With exception of the 0_2^+ state, this shell model calculation gave a very good spectrum to 20 MeV excitation.
- ^{16}O : For this nucleus, we have used the structure as determined by Haxton and Johnson [19]. That was a $(0+2+4)\hbar\omega$ calculation made using a hybrid interaction based upon the $0p$ -shell Cohen and Kurath [20] potentials. The (positive parity) spectrum of ^{16}O to about 10 MeV excitation is quite well reproduced.
- ^{40}Ca : The ground state structure for this nucleus was taken from recent studies [7, 21] made using the SHF(SKX) model of structure. That model lead to better fits to the 200 MeV data (which we consider again herein) than either the simple $0\hbar\omega$ shell model or SHF results made with other interactions.
- ^{90}Zr : For this nucleus, a shell model space defined in the $1p_{\frac{3}{2}}, 0f_{\frac{5}{2}}, 1p_{\frac{1}{2}}, 0g_{\frac{7}{2}}$ orbits was used with the NIS interaction [22]. That interaction was optimized to describe nuclei in the Ni \rightarrow Sn mass region.
- ^{208}Pb : This ground state of this nucleus also is described by a SHF calculation. In this case, using the SKM* interaction [7], wave functions and OBDME (shell occupancies) result with which the 40, 65, and 200 MeV proton elastic differential cross sections as well as the electron scattering form factor have been extremely well reproduced [21].

As noted before [2], with all details preset, the g -folding approach is predictive. So only one calculation of an optical potential and of its use to give cross sections and spin observables is made. How good a reproduction of data results then is a measure of the formulation and/or of the specifications used.

The global Dirac approach [4] is different in philosophy to the above. First it is phenomenological and the functional forms of parameter values were obtained by fitting a large body of data, including most if not all of the data considered herein. From those studies, two parameter sets, which we identify as the *EDAI* (E -dependent A -independent) and *EDAD* (E -dependent A -dependent), specify the Dirac potentials we shall use. From the general form of the model given in Eq. (7), there are eight potentials which are functions of only energy and radius. The *EDAD* fits test the sensitivity of the computation to the input optical model potentials; though there are three different *EDAD* fits [4] that give equally high-quality agreement with the data.

In all figures to follow, results found using the g -folding, the *EDAI*, and the *EDAD3* models will be displayed by the solid, long-dashed, and dot-dashed curves respectively.

A. Cross sections and spin observables: angular variations.

The differential cross sections for 65 MeV and 200 MeV protons elastically scattered from ^{12}C , ^{16}O , ^{40}Ca , ^{90}Zr , and ^{208}Pb are shown in Figs. 1 and 2 respectively. The calculated results are compared with data in nine of the ten cases. The data are displayed by different symbols: filled circles for ^{12}C , open squares for ^{16}O , open diamonds for ^{40}Ca , crosses for ^{90}Zr , and open circles for ^{208}Pb . With all results and data scaled for clarity, from the top down in Figs. 1 are the results and data for ^{12}C (1), ^{16}O (10^{-1}), ^{40}Ca (10^{-2}), ^{90}Zr (10^{-3}), and ^{208}Pb (10^{-5}). The scales used are given in brackets following the target symbol.

Clearly both global DP results fit the data very well as the studies to determine the global set were designed to do. The g -folding results, by comparison, do not do as well. But recall that each g -folding result is a prediction built upon a given microscopic model of the target structure and an effective interaction determined from infinite matter solutions of the NN g -matrices. As such, these results also are very good, predicting reasonable structures and essentially the correct magnitudes for all cases. The structures of the g -folding results are sharper than those of the data suggesting that the absorptive character of the g -folding optical potentials at 65 MeV may be a little weak.

Such is far less the case with the 200 MeV results which are displayed in Fig. 2. In this figure the notation is as for Fig. 1 with now the scale for the ^{208}Pb results (lowest in the diagram) being 10^{-4} . Again both of the global DP cross sections give very good fits to the data while now the g -folding predictions are good representations of that data though with some noticeable disparities at the larger scattering angles; where the magnitudes of the cross sections are less than 0.1 mb/sr and the momentum transfer values are in excess of ~ 2.5 fm $^{-1}$. For such conditions, the first order theory upon which the g -folding model is built may be too limited [2].

The comparisons between data and calculated results for the spin observables are displayed in Figs. 3, 4, 5, and 6. In the first two results for analyzing powers A_y are displayed, while in the latter, two spin polarizations Q are presented. The results for 65 MeV and 200 MeV are shown on the left and right respectively in each figure. The available data are presented by the diverse symbols in each diagram while the calculated results are displayed by the curves. The notation is as specified previously. In Fig. 3, the analyzing powers from

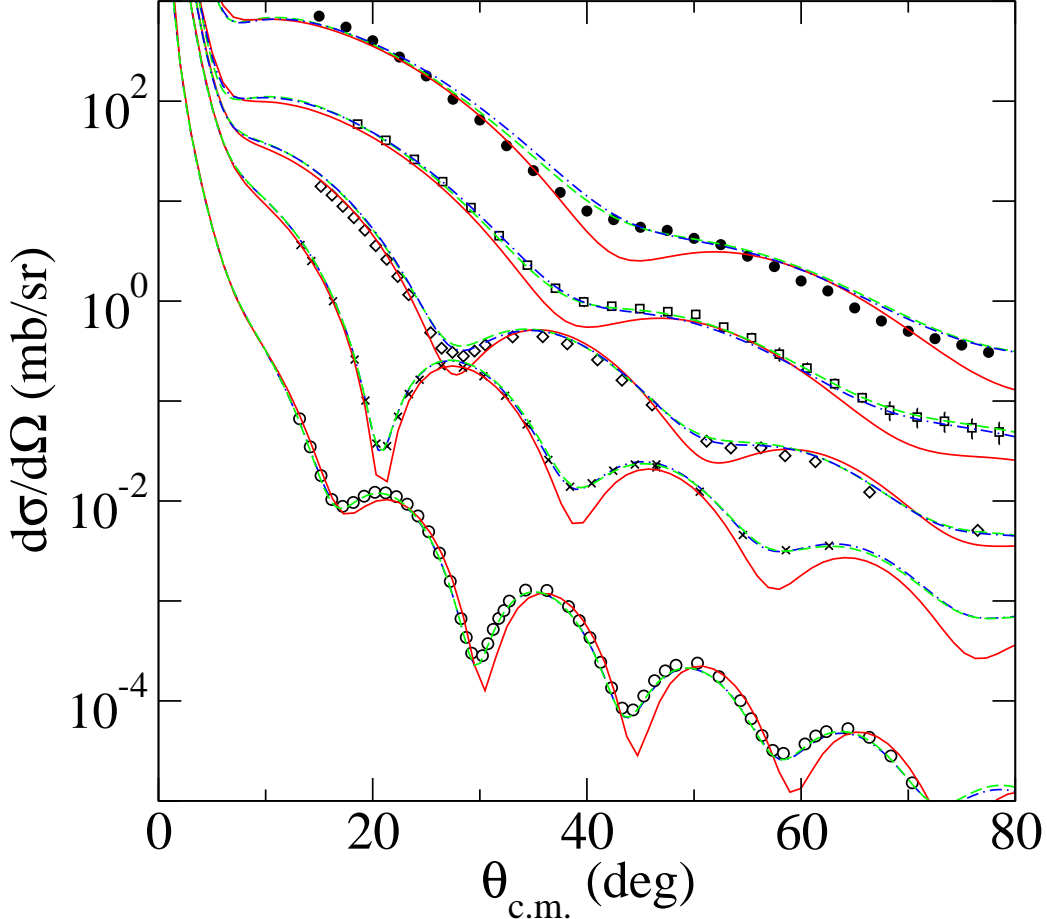


FIG. 1: (Colour online) The differential cross sections from the scattering of 65 MeV protons from five nuclei. Data [23, 24, 25] are compared with the results of different theoretical model calculations. Details are given in the text.

elastic scattering of 65 MeV and 200 MeV protons from ^{12}C , ^{16}O , and ^{40}Ca are shown. Those from ^{90}Zr and ^{208}Pb are presented in Fig. 4. Once more the global DP calculations lead to very good fits to most of these data.

Disparities between the *EDAI* and *EDAD3* results, and between those results and data, are evident at large scattering angles for the ^{12}C and ^{16}O cases. But, as noted before, those regions involve high momentum transfer and very small cross-section values; features that are hardest to fit within a global parameter scheme, let alone with a *g*-folding approach. Of course, if each target is treated independently then it should be possible to find better phenomenological fits to these higher momentum transfer data. As with the cross sections, the predictions obtained with the *g*-folding approach, while not reproducing the data as well as the global DP, still are quite good in comparison with the data. In some cases, the *g*-folding predictions are very good fits. Overall then, the ingredients used in the *g*-folding method can be considered quite realistic.

The spin rotations Q resulting from the three calculations are compared in Figs. 5 and 6. There are very little data available, but that for ^{208}Pb is shown. All three calculated results agree very well with that (limited) data set. For the other nuclei, the global DP results are quite similar, diverging from each similarly to the differences between the analyzing power

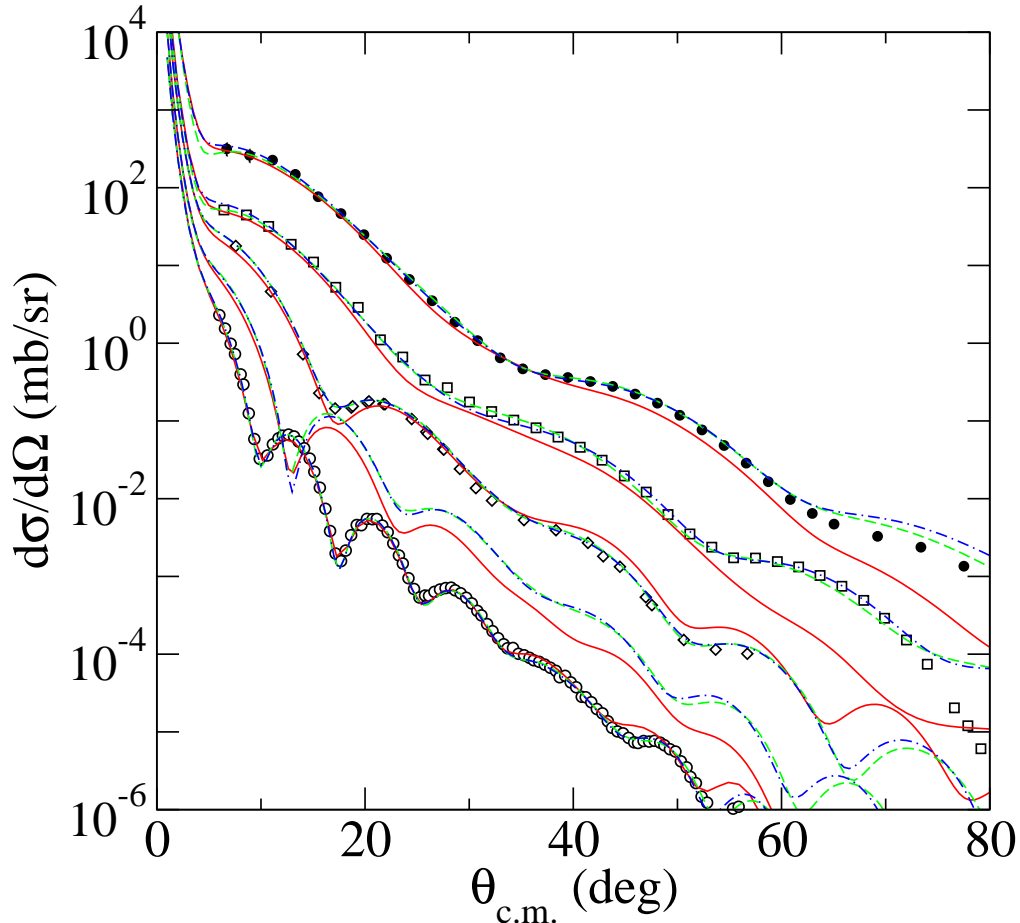


FIG. 2: (Colour online) The differential cross sections from the scattering of 200 MeV protons from five nuclei. Data [26, 27, 28] are compared with the results of different theoretical model calculations. Details are given in the text.

results. They also differ from the g -folding results in like fashion. As with the comparisons of analyzing powers, the spin rotations from all three calculations are in quite good agreement structurally to over 40° in the center of mass.

B. Total reaction and total cross section results

1. Proton total reaction cross sections

In this subsection predictions of the total reaction cross sections for proton scattering are displayed. Results for energies to 800 MeV for the five nuclei considered are compared against data; the latter taken from many sources as listed in Table I.

The results for scattering from ^{12}C are presented in Fig. 7. Total proton reaction cross sections are shown for a projectile energy range from 20 MeV to 900 MeV. Although experimental data exist to much lower energies, any effective mean field prescription for the optical potential at such low energies is not appropriate. However, in a recent paper [52], a multi-channel algebraic scattering (MCAS) theory has been developed with which the low

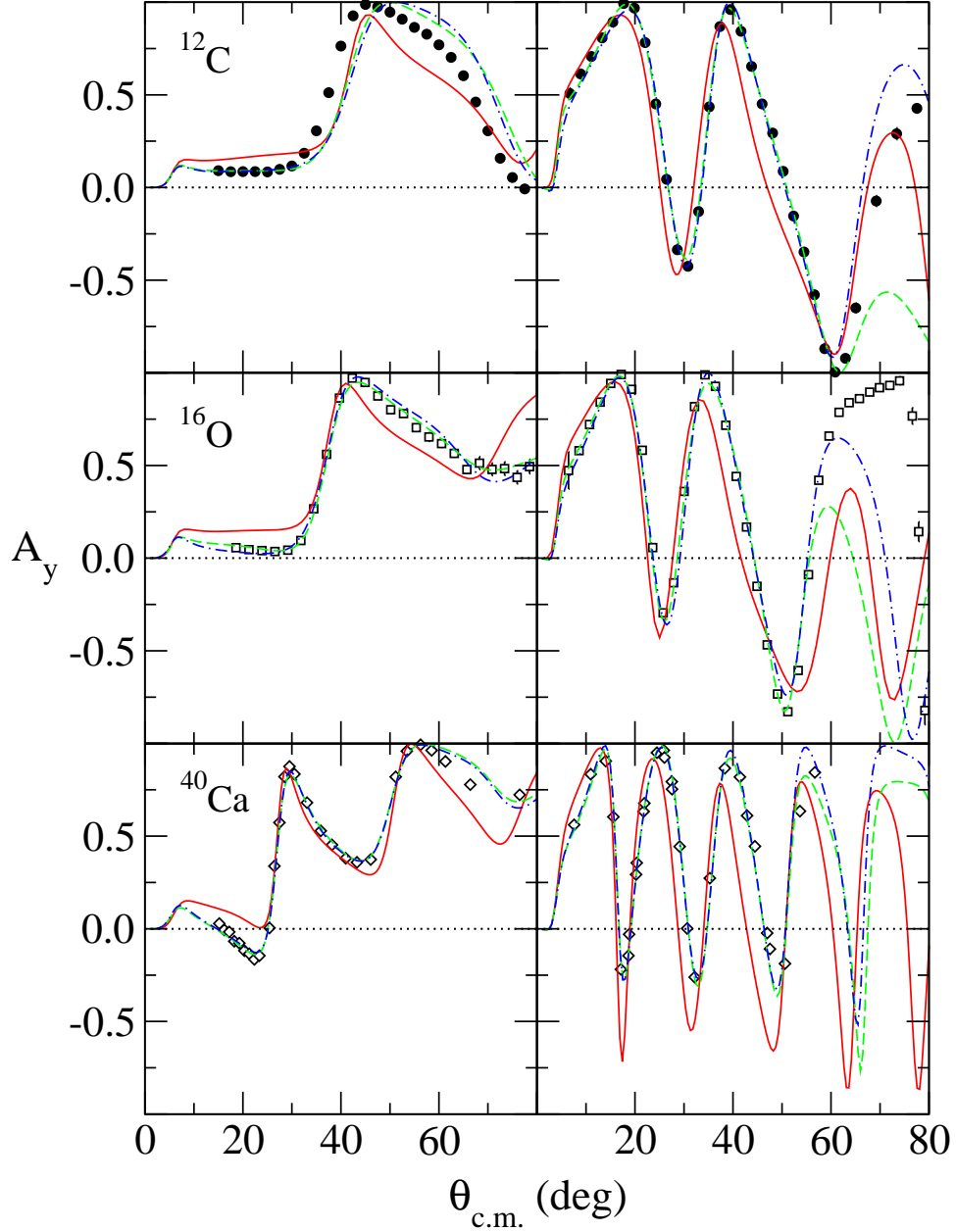


FIG. 3: (Colour online) Analyzing powers from 65 (left) and 200 (right) MeV proton elastic scattering from ^{12}C (top), ^{16}O (middle), and ^{40}Ca (bottom). Details are given in the text.

TABLE I: Sources of proton reaction cross-section data.

Nucleus	Proton references (in year order)
^{12}C	[29], [30], [31], [32], [33], [34], [35], [36], [37], [38], [39], [40], [41], [42], [43]
^{16}O	[44], [40], [45]
^{40}Ca	[34], [46], [38], [47], [45], [43]
^{90}Zr	[48], [38], [49], [39]
^{208}Pb	[30], [32], [33], [35], [46], [50], [38], [39], [40], [51], [45], [43]

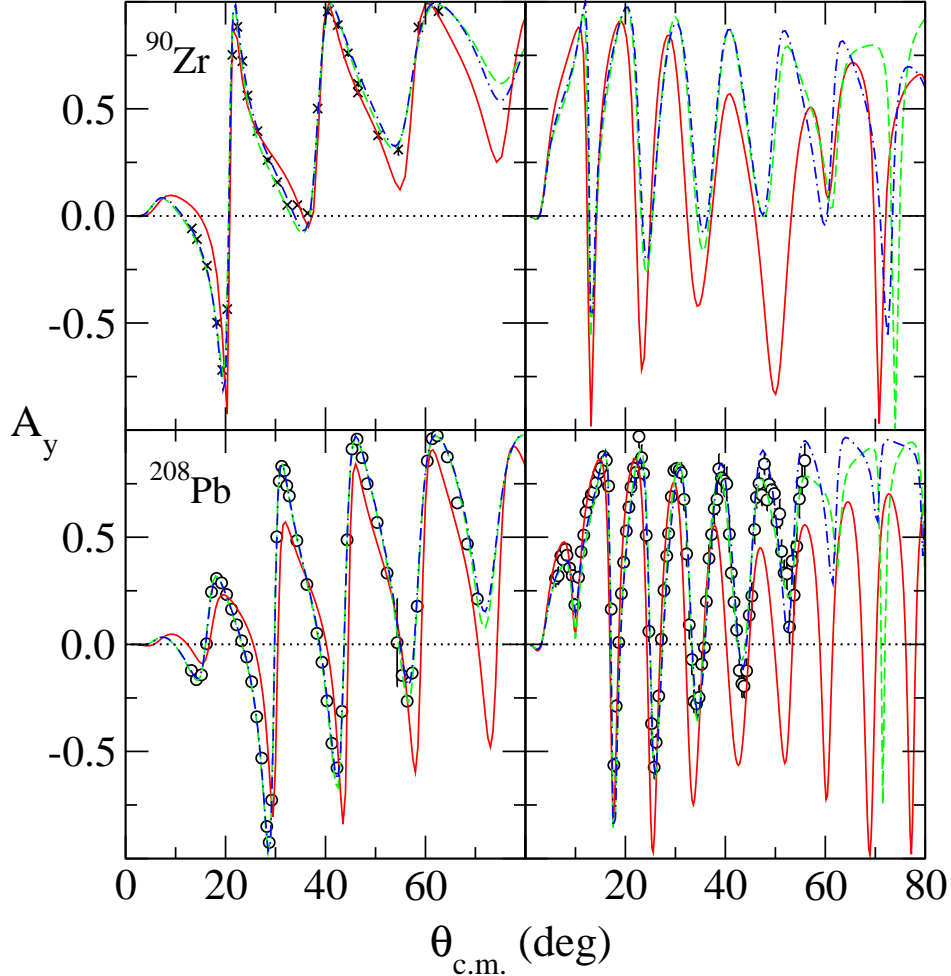


FIG. 4: (Colour online) Analyzing powers from 65 (left) and 200 (right) MeV proton elastic scattering from ^{90}Zr (top) and ^{208}Pb (bottom). Details are given in the text.

energy range should be covered. This MCAS approach lends itself to specification of the dynamic polarization potential resulting from a summation over all diverse channel functions allowed in that theory. But the resultant optical potential then is extremely non-local and energy dependent; as it need be not only to produce a smooth energy varying elastic scattering cross section but also to give the sharp and broad resonances readily observed at low (< 20 MeV) energies [52]. The low level densities in most spectra to ~ 20 MeV is not a condition conducive to confidence in the g -folding or any mean field optical model potentials. Nonetheless for ^{12}C , there are many data points at energies between 20 and 40 MeV and a significant number thereafter to 500 MeV. Above that there are only a few.

In Fig. 7, the data to 300 MeV are well reproduced by the g -folding model results. But for the higher energies, the g -folding approach is inadequate; seriously under-predicting the data. That is the case for all five targets emphasizing the energy regime limit one need remember for this microscopic Schrödinger approach to scattering. On the other hand the reaction cross sections determined with both the *EDAI* and *EDAD3* global potentials reflect the data very well falling within the uncertainties at most energies. Some data, notably at 61 MeV [33] and at 77 MeV [35] are in disagreement with all three calculated

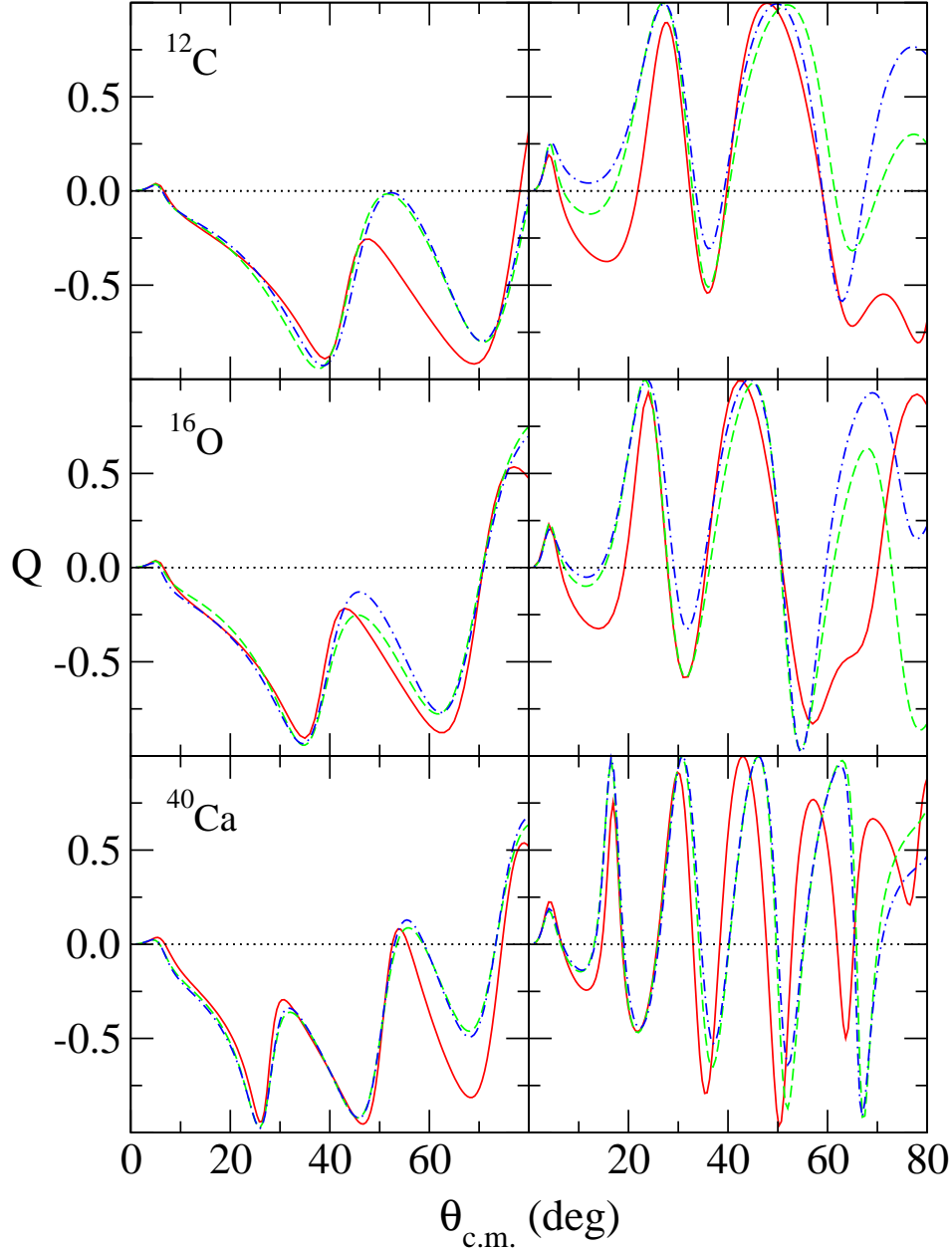


FIG. 5: (Colour online) Spin rotations from 65 (left) and 200 (right) MeV proton elastic scattering from ^{12}C (top), ^{16}O (middle), and ^{40}Ca (bottom). Details are given in the text.

results. However, they are exceptional points in that they also disagree with empirical values taken at nearby energies. Menet *et al.* [39] argue that a much larger systematic error should have been used in the data processing of earlier experiments that lead to the exceptional points. Such also occur with data taken on other targets.

Predictions for proton scattering from ^{16}O are compared with data in Fig. 8. There is no $p\text{-}^{16}\text{O}$ total reaction cross section data for energies between 50 MeV and 200 MeV. Nonetheless the g -folding potential predictions to 50 MeV are in very good agreement with data for those energies. But as with the case of ^{12}C , the g -folding approach under-predicted the four data points in the energy range 200 MeV and 600 MeV. These high energy data are

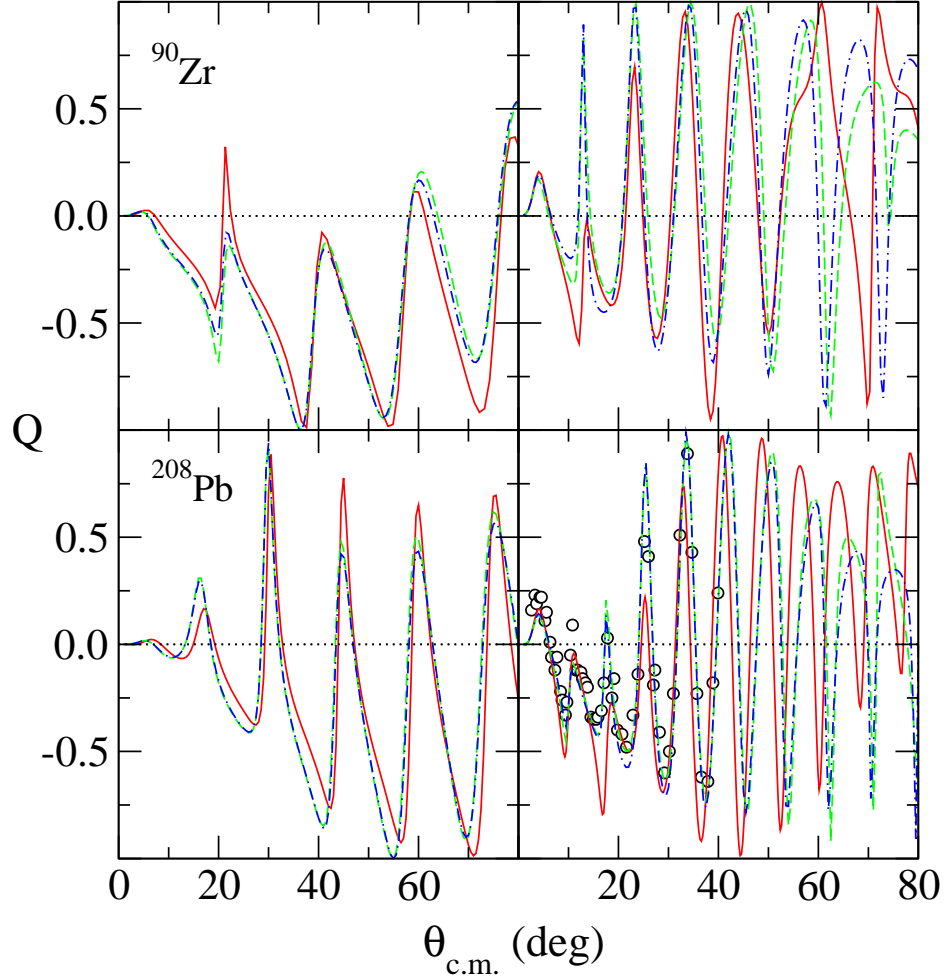


FIG. 6: (Colour online) Spin rotations from 65 (left) and 200 (right) MeV proton elastic scattering from ^{90}Zr (top) and ^{208}Pb (bottom). Details are given in the text.

well replicated by the global DP potentials however, and by the *EDAD3* model in particular. That model also gave results that compare well the data at lower energies while the *EDAI* result over-predicted them.

Predictions for proton scattering from ^{40}Ca are compared with data in Fig. 9. There are relatively few data points in the energy range with but one (at 700 MeV) above 180 MeV. Again the predictions made using the g -folding potentials are in very good agreement with the data for energies to 180 MeV. But the microscopic approach underestimates the datum at 700 MeV. Both the global DP (*EDAI* and *EDAD3*) models replicate the data well at the energies to 65 MeV, overestimate the data at the energies near 100 MeV and 180 MeV, and reproduce very well the datum at 700 MeV.

In Fig. 10, we present the data and our predictions of the total reaction cross sections for proton scattering from ^{90}Zr . There is very little data with which to compare, nevertheless the g -folding potential gives results in very good agreement with the five actual data points in the energy range 30 to 100 MeV. On the other hand both global DP model calculations slightly overestimate that data set. Again however, it is in the higher energy ranges that the g -folding and Dirac model predictions diverge, as we have come to expect.

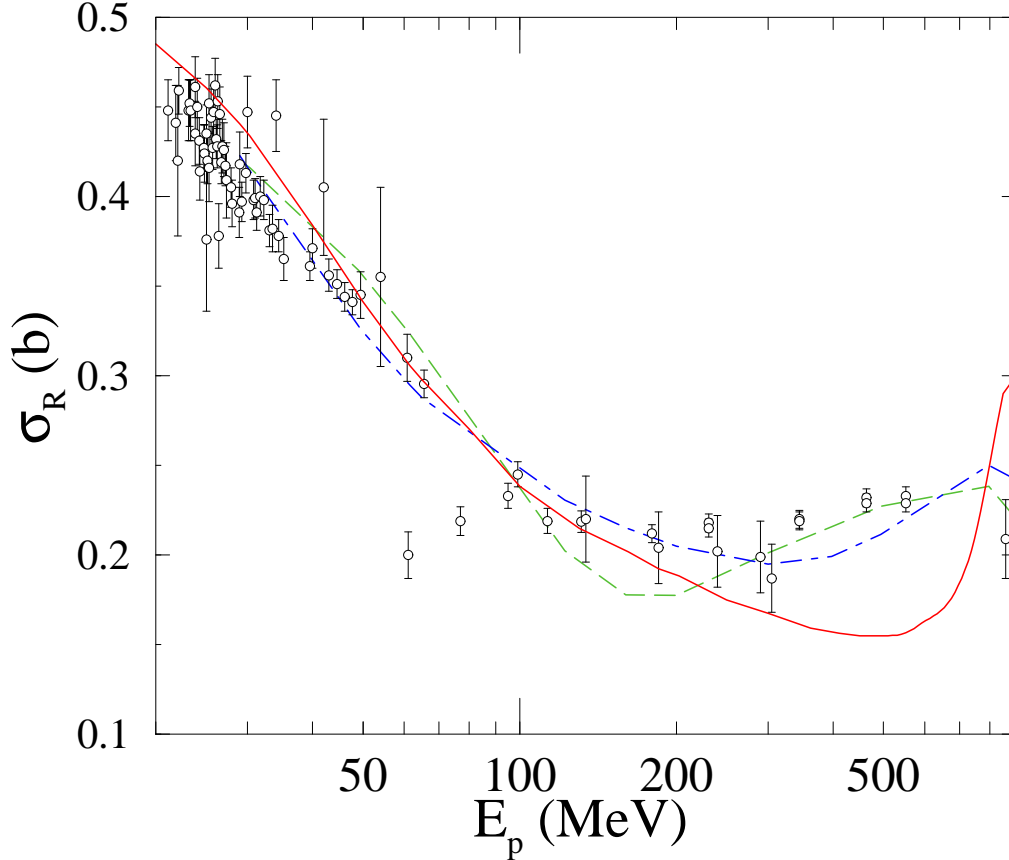


FIG. 7: (Colour online) Energy variation of σ_R for proton scattering from ^{12}C . The curves are identified in the text while data references are as given in Table I.

In Fig. 11, we compare the calculated total proton reaction cross sections from ^{208}Pb with data taken from the references listed in Table I. For this nucleus, the data are quite scattered with some being quite disparate. In this case the g -folding model calculations underestimate data at energies between 20 MeV and 40 MeV but agree well with the data taken at energies thereafter to 300 MeV. On the other hand, both *EDAI* and *EDAD3* global DP models reproduce a select set of the data over the whole energy range quite well. As with ^{12}C , exceptional data points are found near 30 MeV, 61 MeV and 77 MeV. In this case, other data from ^{208}Pb taken at 60.8 MeV [39] and 65.5 MeV [43] give different results and in fact are values of reaction cross sections that are in accord with our model predictions.

2. Energy variations of neutron total cross sections

Accurate measurements of neutron total reaction cross sections are far more difficult to achieve than their proton counterparts. Indeed usually those cross sections are obtained by subtracting the elastic from the total scattering cross section. While both of those cross sections can be measured with some accuracy, the subtraction of two large numbers with attendant uncertainties compounds uncertainty in the result. We note, however, that a new Japanese technique, for measuring neutron total reaction cross sections utilizing in-beam and

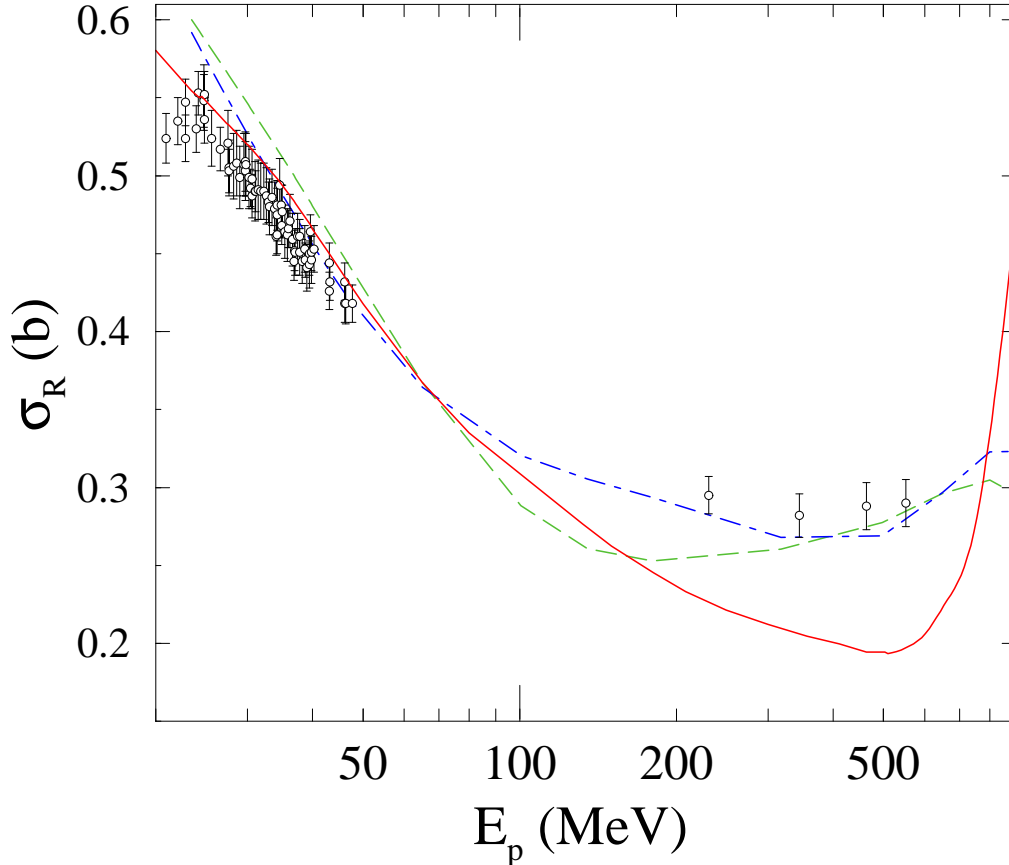


FIG. 8: (Colour online) Energy variation of σ_R for proton scattering from ^{16}O . The notation is as in the text.

out-beam methods similar to those used in proton scattering, shows promise. Nevertheless, herein, we concentrate on analyses of total scattering cross-section data.

The data we have chosen to analyze have been taken from a recent survey by Abfalterer *et al.* [53]. That survey includes data measured at LANSCE that are supplementary and additional to those published earlier by Finlay *et al.* [54]. For comparison with that recent data compilation, we calculate neutron total scattering cross sections for the five nuclei of interest; ^{12}C , ^{16}O , ^{40}Ca , ^{90}Zr , and ^{208}Pb .

In forming neutron optical potentials by the g -folding method, we have used the same structure models and effective NN interactions chosen to create the proton optical potentials whose results were presented and discussed above. Likewise global DP model potentials for neutrons were formed using the *EDAI* and *EDAD3* parameter sets that have been used to get proton scattering results, and with the Coulomb potential set to zero, generated results displayed and discussed. No Coulomb energy shift has been made in those calculations. Thus all of the results shown in Fig. 12 are predictions. For ^{12}C , neutron total cross sections are well predicted by all three model calculations. The *EDAI* and *EDAD3* potentials of the global DP give very good results for energies above 20 MeV, while the g -folding model calculations do so for energies between 50 MeV and 300 MeV. Outside of that range the g -folding results under-predict data. Below 20 MeV in this case, as well as for ^{16}O which is considered next, resonance effects are very evident. Such are not encompassed in the

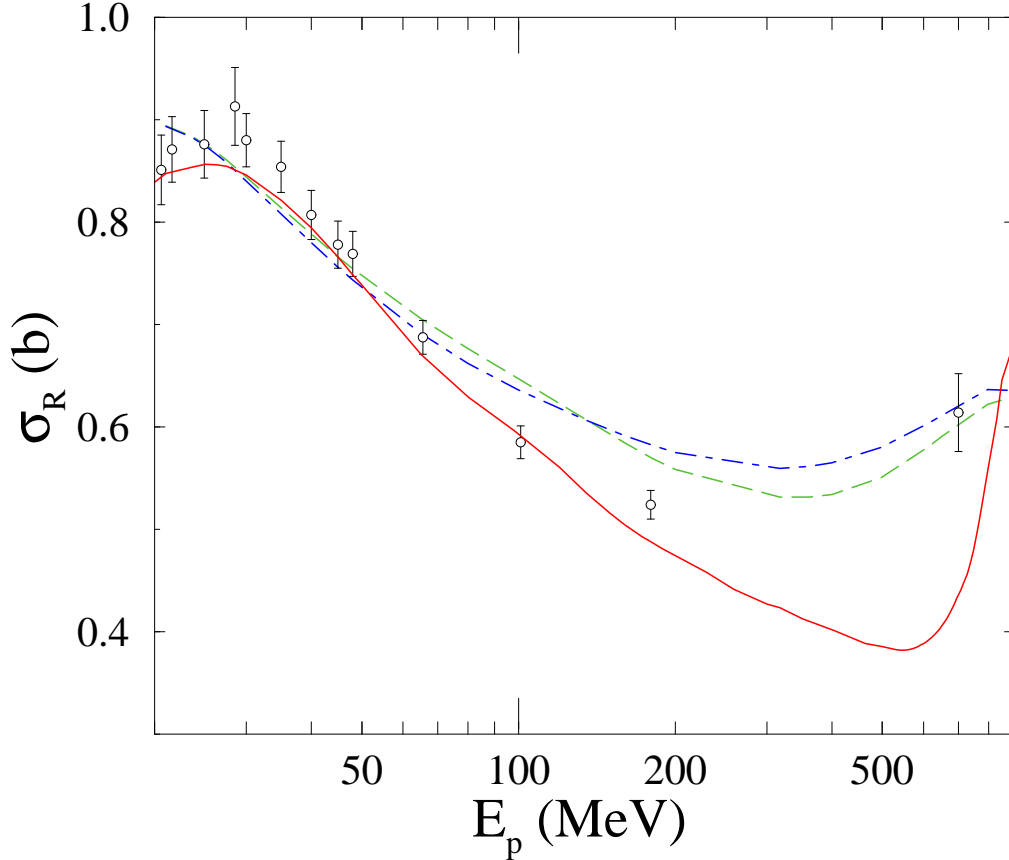


FIG. 9: (Colour online) Energy dependencies of σ_R for proton scattering from ^{40}Ca . The notation is as in the text.

mean field models we consider. For ^{16}O , the model results follow a similar pattern as for ^{12}C . Global DP results give good fits to the data as does the g -folding model but only for energies above ~ 70 MeV. The $EDAD3$ model predicts well data for the whole energy range while the $EDAI$ model slightly over-predicts data between 20 MeV and 60 MeV.

For the three heavier nuclei, ^{40}Ca , ^{90}Zr , and ^{208}Pb , the total cross sections down to 10 MeV do not show significant resonance features but there is the onset of a Ramsauer-like effect which accentuates with target mass. None of the models predict such large scale oscillations adequately, though with improved structure details, as used in the calculations for scattering from ^{208}Pb , those oscillations are more noticeable when compared to results from use of a simple oscillator model of structure [55]. The results found for these three nuclei show a degradation in the quality of the predictions from all three model calculations. For ^{40}Ca , the comparisons are still similar to what is noticed for the lighter mass targets, though the g -folding model predictions above 300 MeV are poorer. For ^{90}Zr and ^{208}Pb all three model results clearly depart from what is observed. However, the g -folding results trend quite well as average results upon which a Ramsauer effect may be superimposed [56].

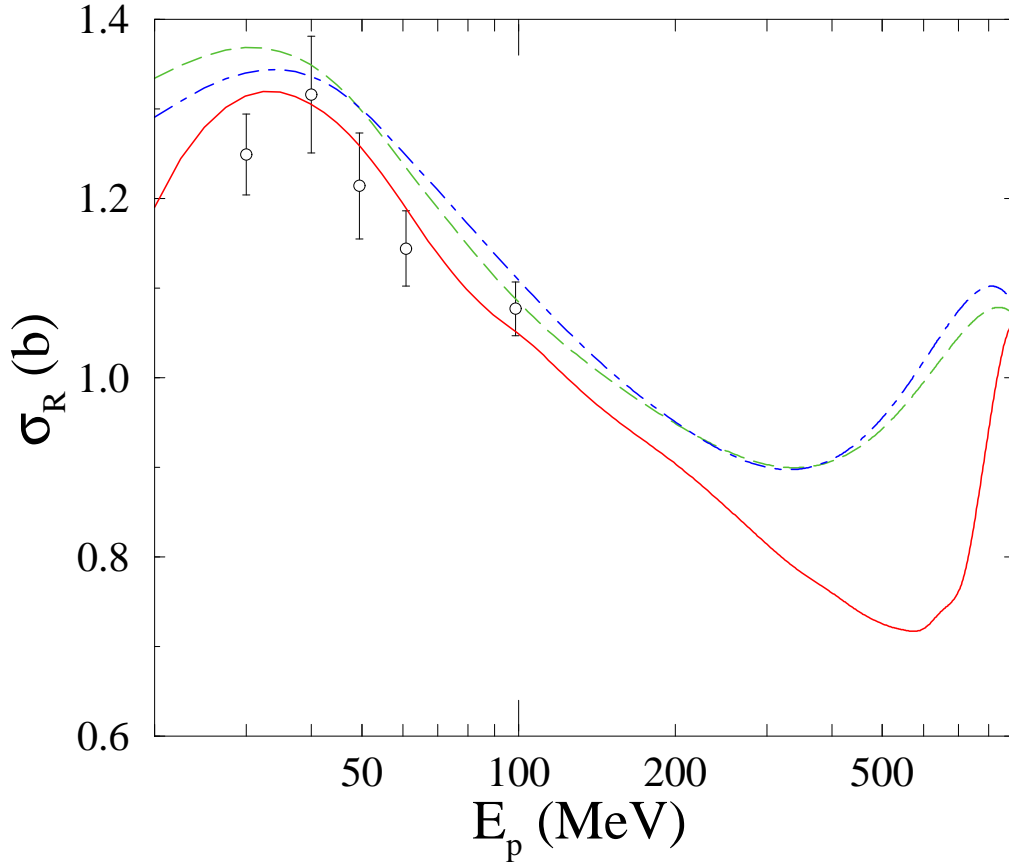


FIG. 10: (Colour online) Energy dependencies of σ_R for proton scattering from ^{90}Zr . Basic notation is as for Fig. 7.

IV. CONCLUSIONS

A microscopic coordinate space Schrödinger model of nucleon-nucleus interactions and global DP model for the same systems, have been used to predict proton and neutron scattering cross sections; both angular and integral. Cross-section data and spin observables have been well described for energies at which the diverse models are valid. That includes a substantial range of energies in common for both approaches.

Our first study was of angular dependent observables; differential cross sections and spin observables (analyzing powers and spin rotations) for elastic proton scattering at 65 MeV and at 200 MeV. Both methods of analysis gave good reproduction of measured data. The two models, with the global DP potentials defined from the parameter specifications in the recent study of their energy and mass dependences [4], were used to predict proton total reaction and neutron total cross sections in scattering from five nuclei, ^{12}C , ^{16}O , ^{40}Ca , ^{90}Zr , and ^{208}Pb . Both models gave good predictions of that data (in the energy regimes for which the models are appropriate) with the largest discrepancies reflecting the Ramsauer effect in neutron total cross sections.

Fundamentally, our Dirac and Schrödinger approaches are different. The microscopic Schrödinger model incorporates all the dominant medium modifications in the optical potential, without significant approximation, by using a realistic ground state density to give

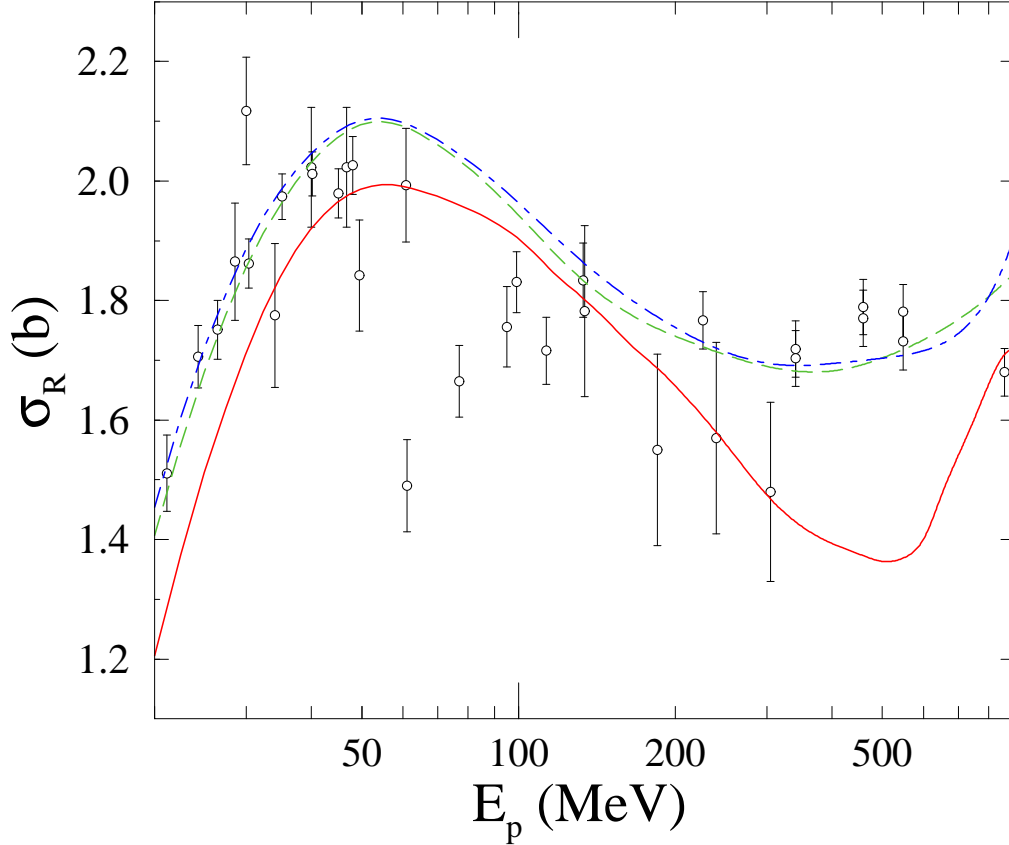


FIG. 11: (Colour online) Energy dependencies of σ_R for proton scattering from ^{208}Pb . The notation is as in the text.

a reasonable specification of all terms in the optical potential. The global DP approach provides a natural specification of such terms in local equivalent form. Nonetheless, the comparisons obtained in this work are exemplary of the dilemma in judging the relative merits of relativistic *vs.* non-relativistic approaches for the analyses of intermediate energy nucleon-nucleus scattering. That the two models give results that agree so well for the differential cross sections as well as for both spin observables and for both projectiles gives confidence in the reality of calculated results at the two energies we considered. As has been speculated [1] however, the answer throughout the energy regime may lie in QCD-based models of nuclear scattering systems. Indeed the work of Cohen *et al.* [57] shows evidence that the large scalar and vector fields of Dirac Phenomenology may be related to quark degrees of freedom in the nucleon. However, such QCD-based theoretical models and concomitant experiments will require simultaneous treatment of proton and neutron scattering in order to be complete. Sadly, the latter's experimental database currently is lacking.

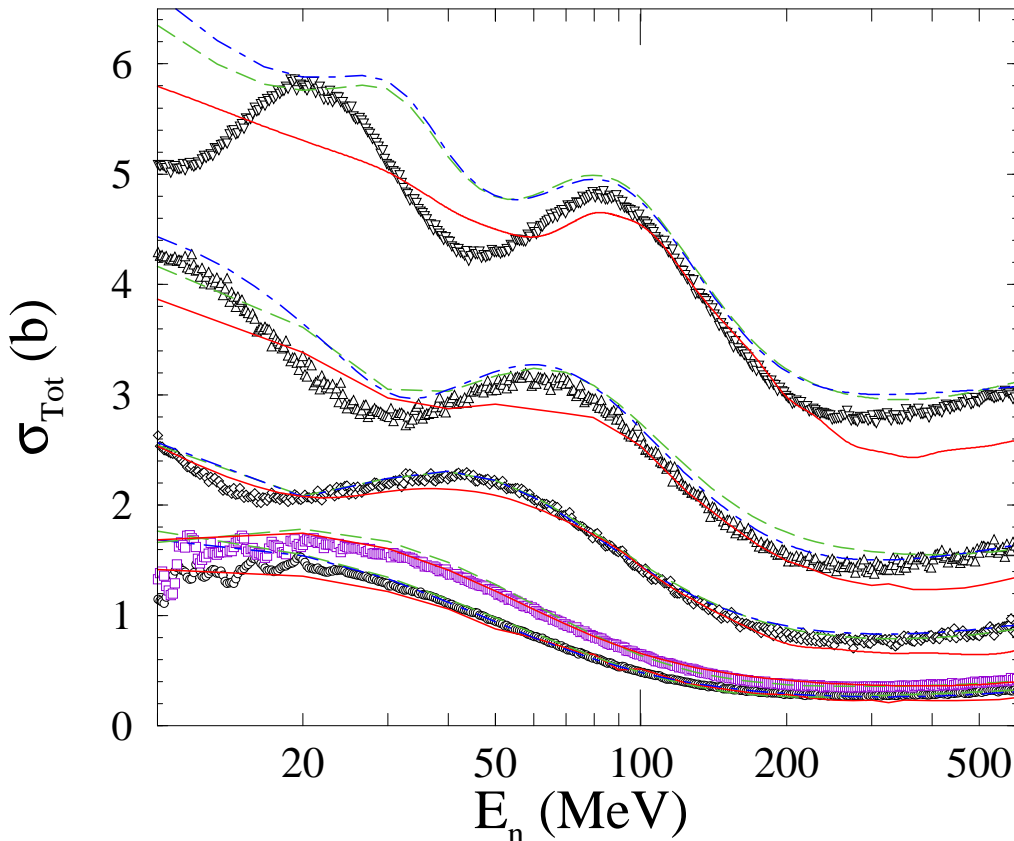


FIG. 12: (Colour online) Total cross sections for neutrons scattered from ^{12}C , ^{16}O , ^{40}Ca , ^{90}Zr , and ^{208}Pb . The data are those of Abfalterer *et al.* [53]; for ^{12}C the data correspond to scattering from natural carbon.

Acknowledgments

This research was supported by the National Science Foundation under Grant No. 0098645 and by a research grant from the Australian Research Council.

-
- [1] L. Ray, G. W. Hoffmann, and W. R. Coker, *Phys. Rep.* **212**, 223 (1992), and references cited therein.
 - [2] K. Amos, P. J. Dortmans, H. V. von Geramb, S. Karataglidis, and J. Raynal, *Adv. in Nucl. Phys.* **25**, 275 (2000), and references cited therein.
 - [3] B. D. Serot and J. D. Walecka, *Adv. Nucl. Phys.* **16**, 1 (1986), and references cited therein.
 - [4] E. D. Cooper, S. Hama, B. C. Clark, and R. L. Mercer, *Phys. Rev. C* **47**, 297 (1993), and references cited therein.
 - [5] R. Kozack and D. G. Madland, *Phys. Rev. C* **39**, 1461 (1989).
 - [6] P. K. Deb, K. Amos, S. Karataglidis, M. B. Chadwick, and D. G. Madland, *Phys. Rev. Lett.* **86**, 3248 (2001).
 - [7] B. A. Brown, *Phys. Rev. Lett.* **85**, 5296 (2000).

- [8] B. Friedman and V. R. Pandharipande, Nucl. Phys. **A361**, 502 (1981).
- [9] B. C. Clark, L. J. Kerr, and S. Hama, Phys. Rev. C **67**, 054605 (2003), and references cited therein.
- [10] S. Karataglidis and D. G. Madland (2001), nucl-th/0103048.
- [11] A. J. Koning and J. P. Delaroche, Nucl. Phys. **A713**, 231 (2003).
- [12] R. Machleidt, K. Holinde, and C. Elster, Phys. Rep. **149**, 1 (1987).
- [13] J. Raynal, *computer code dwba98* (1999), (NEA 1209/05).
- [14] B. C. Clark, S. Hama, S. G. Kälbermann, E. D. Cooper, and R. L. Mercer, Phys. Rev. C **31**, 694 (1985).
- [15] E. D. Cooper and B. K. Jennings, Nucl. Phys. **A483**, 601 (1988).
- [16] R. H. Landau, *Quantum Mechanics II, A Second Course in Quantum Theory* (Wiley, New York, 1990).
- [17] S. Karataglidis, P. J. Dortmans, K. Amos, and R. de Swiniarski, Phys. Rev. C **52**, 861 (1995).
- [18] E. K. Warburton and B. A. Brown, Phys. Rev. C **46**, 923 (1992).
- [19] W. C. Haxton and C. Johnson, Phys. Rev. Lett **65**, 1325 (1990).
- [20] S. Cohen and D. Kurath, Nucl. Phys. **73**, 1 (1965).
- [21] S. Karataglidis, K. Amos, B. A. Brown, and P. K. Deb, Phys. Rev. C **65**, 044306 (2002), and references cited therein.
- [22] X. Ji and B. H. Wildenthal, Phys. Rev. C **40**, 389 (1989).
- [23] T. Noro et al., Nucl. Phys. **A366**, 189 (1981).
- [24] H. Sakaguchi et al., Phys. Rev. C **26**, 944 (1982).
- [25] S. Kato et al., Phys. Rev. C **31**, 1616 (1985).
- [26] J. R. Comfort, G. L. Moake, C. C. Foster, P. Schwandt, and W. G. Love, Phys. Rev. C **26**, 1800 (1982).
- [27] H. Siefert et al., Phys. Rev. C **47**, 1615 (1993).
- [28] D. A. Hutcheon et al., in *AIP conf. Proc. No. 69*, edited by G. G. Ohlson, R. E. Brown, N. Jarmie, W. W. McNaughton, and G. M. Hale (AIP, New York, 1981).
- [29] G. P. Millburn, W. Birnbaum, W. E. Crandall, and L. Schecter, Phys. Rev. **95**, 1268 (1954).
- [30] J. M. Cassels and J. D. Lawson, Proc. Phys. Soc. (London) **A67**, 125 (1954).
- [31] E. J. Burge, Nucl. Phys. **13**, 511 (1959).
- [32] T. J. Gooding, Nucl. Phys. **12**, 241 (1959).
- [33] V. Meyer, R. M. Eisberg, and R. F. Carlson, Phys. Rev. **117**, 1334 (1960).
- [34] A. Johansson, U. Svanberg, and O. Sundberg, Arkiv Fysik **19**, 527 (1961).
- [35] R. Goloskie and K. Strauch, Nucl. Phys. **29**, 474 (1962).
- [36] R. A. Giles and E. J. Burge, Nucl. Phys. **50**, 327 (1954).
- [37] M. Q. Makino, C. N. Waddell, and R. M. Eisberg, Nucl. Phys. **50**, 145 (1964).
- [38] P. Kirkby and W. T. Link, Can. J. Phys. **44**, 1847 (1966).
- [39] J. J. H. Menet, E. E. Gross, J. J. Malanify, and A. Zucker, Phys. Rev. C **4**, 1114 (1971).
- [40] P. U. Renberg, D. F. Measday, M. Pepin, P. Schwaller, B. Favier, and C. Richard-Serre, Nucl. Phys. **A183**, 81 (1972).
- [41] W. F. McGill et al., Phys. Rev. C **10**, 2237 (1974).
- [42] I. Slaus, D. J. Margaziotis, R. F. Carlson, W. T. H. van Oers, and J. R. Richardson, Phys. Rev. C **12**, 1093 (1975).
- [43] A. Ingemarsson et al., Nucl. Phys. **A653**, 341 (1999).
- [44] R. Chapman and A. M. Macleod, Nucl. Phys. **A94**, 313 (1967).
- [45] R. F. Carlson et al., Phys. Rev. C **12**, 1167 (1975).

- [46] J. F. Turner, B. W. Ridley, P. E. Cavanagh, G. A. Gard, and A. G. Hardacre, Nucl. Phys. **58**, 509 (1964).
- [47] J. F. Dicello and G. Igo, Phys. Rev. C **2**, 488 (1970).
- [48] B. D. Wilkins and G. Igo, Phys. Rev. **129**, 2198 (1963).
- [49] J. F. Dicello, G. J. Igo, and M. L. Roush, Phys. Rev. **157**, 1001 (1967).
- [50] R. E. Pollock and G. Schrank, Phys. Rev. **140**, B575 (1965).
- [51] D. G. Montague, R. K. Cole, M. Makino, and C. N. Waddell, Nucl. Phys. **A199**, 457 (1973).
- [52] K. Amos, L. Canton, G. Pisent, J. P. Svenne, and D. van der Knijff, Nucl. Phys. **A728**, 65 (2003).
- [53] W. P. Abfalterer, F. B. Bateman, F. S. Dietrich, R. W. Finaly, R. C. Haight, and G. L. Morgan, Phys. Rev. C **63**, 044608 (2001).
- [54] R. W. Finlay, W. P. Abfalterer, G. Fink, E. Montei, T. Adami, P. W. Lisowski, G. L. Morgan, and R. C. Haight, Phys. Rev. C **47**, 237 (1993).
- [55] K. Amos, S. Karataglidis, and P. K. Deb, Phys. Rev. C **65**, 064618 (2002).
- [56] P. K. Deb, K. Amos, and S. Karataglidis, Phys. Rev. C **70**, 057601 (2004).
- [57] T. D. Cohen, R. J. Furnstahl, and D. K. Griegel, Phys. Rev. Lett. **67**, 961 (1991).